A Numerical Optimization Framework for Rotor Airfoil Design

Gunther Wilke
Institute of Aerodynamics and Flow Technolgy
German Aerospace Center (DLR) Braunschweig
Lilienthalplatz 7, 38106 Braunschweig, Germany

Abstract

The design of new helicopter airfoils is a challenging task. The individual blade sections undergo very different flow conditions during the various flight regimes of the helicopter. In forward flight, the advancing side operates in a transonic regime where potentially shock waves can occur, while on the retreating side little flow velocities at high angle of attacks are seen up to reverse flow. In hover, the oncoming tip vortex of the previous blade drastically influences the inflow on the rotor. Therefore, after a brief review of given design techniques, a novel approach for airfoil designs is put forward. A surrogate based multi-objective approach including constraints is utilized to concurrently optimize an airfoil for hover, retreating and advancing side flow, while also enforcing a certain robustness as to not looking at single design points in these global flow regimes. Along with the estimation of design targets, this 2D flow analysis-based framework allowed to optimize the airfoil design of an existing model rotor blade. A comparison over a range of flight conditions of the rotor with and without the new airfoils proved the validity of this approach.

Keywords: robust airfoil design, NACA23012, HART-II, OA209, multi-objective surrogate-based optimization

1 INTRODUCTION

The design of airfoils for helicopters is a challenging task as the flow field around the rotor blades varies greatly. In contrast to fixed-wing aircraft which deploy slats and flaps to adjust the airfoil to the specific flight condition, this sort of devices have not been established yet on mass produced helicopters. Thus, rotor airfoils must perform well in high speed transonic flow, while also being able to still generate lift in almost incompressible flows.

A common approach for airfoil design is the two-dimensional analysis to guide the designer towards a better design through panel methods or Euler codes coupled boundary layer analysis, such as XFOIL [1] or MSES [2] by Drela. These tools allow the designer to look at individual sections of the blade and tailoring each one individually without requiring to take the others into account with an acceptable computational effort. The challenge for helicopter rotors is the determination of the correct inflow states and selection of the most vital ones for the design. Dadone [3] proposes a set of rules for this, where the actual rotor design shall be checked in various flow conditions in order to arrive at a successful design. This is also reflected in the work by Thibert and Gallot [4], who come up with a set of metrics and flow conditions to design the OA209 airfoil. Generally, a reduction of the drag coefficient for the airfoil is desirable, while at the same time a certain maximum lift has to be ensured and the pitching moment is to be limited to avoid structural failure of the rotor. Bousman [5] also derives recommendations for rotor airfoil design based on findings with a comprehensive code.

While the aforementioned design studies were carried out manually, recent approaches take advantage of numerical optimization procedures. While numerical optimization does not relief the airfoil designer of understanding the physics, it may help finding an improved design more quickly by performing parameter studies in a smart way. The full topic of numerical optimization will not be covered here, but the reader is referred to Martins and Ning [6]. The ingredients for a numerical optimization of airfoils is a parameterization technique, an numerical optimization algorithm, and a simulation tool to compute the merits of the tried airfoil designs.

Regarding parameterization techniques, numerous approaches exist. Aside from splining techniques such as Bezier, Cubic and NURB splines [7], Hicks and Henne bump functions [8] as well as the CST parameterization by Kulfan [9] are often employed. They specifically drive the upper and lower surface of the airfoil. Opposing this, parameterization based on the camberline and thickness distribution exist, with the NACA 4 and 5 series parameterizations [10] being the most renowned ones, but derivatives based on this are given for example by Xiaoqiang et al. [11] or Allen et al. [12]. PARSEC by Sobieczky [13] falls in between these two categories. For the optimization, a trade-off has to be made between the number of parameters employed and flexibility. With more parameters, the cost of the optimization will grow, while on the other hand a reduced number of parameters will limit the optimizer in finding a good design. Song and Keane [14] studied the effect of increasing parameters, while Marinus [15] compared the effect of different parameterizations. Both cases also show that undesirable shapes may be obtained if the optimization is too flexible.

For the numerical optimization, two general routes are either fast gradient-based optimization techniques that find the next minimum quickly versus the more expensive heuristic evolutionary approaches that seek the global optimum. The gradient based approaches are often coupled with adjoint CFD solvers, which efficiently compute the gradient. One such example is given by Ilic and Brezillon [16]. Lane [17] uses numerical optimization to find a good airfoil shape using preset pressure distributions known as inverse design. On the other side is the application of evolutionary algorithms often in conjunction with surrogate models to speed up the optimization effort. Obayashi and Takanashi [18] utilize genetic optimization procedures to optimize their pressure distribution to then arrive at the final airfoil shape through inverse design. Koziel and Leifsson [19], Leifsson et al. [20] employ variable-fidelity techniques to further accelerate the surrogate based optimization process of airfoils with global optimizers. Massaro and Andrea [21] optimize rotor airfoils with artificial neural networks and genetic algorithms. Fusi et al. [22] also employ variable-fidelity methods and include uncertainty quantification techniques to obtain robust rotorfoil designs that operate well in multiple flight conditions.

Another way to obtain better airfoils is the direct 3D approach, where the shape of the rotor is altered to improve aspects of the rotor directly. Lee and Kwon [23], or Choi et al. [24] simulate the rotor in hover and calculate the gradient through the adjoint approach to optimize the outer shape of the rotor including the airfoil shapes. Rotor shapes in forward flight have been optimized by Wang et al. [25], or Fabiano et al. [26] using the unsteady adjoint formulation. While a break-through by itself, it nevertheless requires a lot of resources and therefore intermediate approaches exist by Vu et al. [27], Vu and Lee, [28] or Allen et al. [12]. They compute airfoil polars with a 2D analysis code and validate the gains of their designs with their comprehensive codes. The adjoint based as well as the simplified comprehensive code approaches deliver airfoils suited for the specific flight condition, yet the versatility may suffer, as they are limited in the number of flight conditions that can be investigated.

Ahuja et al. [29] and Mani et al. [30] optimize airfoils for dynamic stall. While an achievement by itself, the retrieved airfoils become noticeably thicker and therefore are less suited for transonic flow where shocks may occur. Both works therefore conclude that their findings need to be put into perspective and recommend the application of multi-objective optimization procedures to arrive at more robust airfoil designs as Fusi et al. [22] propose.

DLR has contributed in various airfoil design activities. The recent airfoils designed for helicopter blades have been the EDI-M109 and EDI-M112 airfoils, which were developed jointly with IAG Stuttgart for Airbus helicopters (back then Eurocopter) [31]. During the assoziated project, inverse design competed with a direct numerical optimization at specific flow conditions and regular exchange between the participating parties led to the final designs.

In the scope of the present research, this work aims at a robust design technique based direct analysis coupled with an optimization. Opposed to Fusi et al., who concurrently optimize their airfoil for the mean and standard deviation in a single flow condition, here multiple flow conditions are considered and the mean for a range over lift coefficients is improved, as Fusi et al. propose in the conclusions of their paper.

2 METHODOLOGY

The proposed optimization procedure consists of an optimization strategy, a parameterization of for the airfoil and a simulation approach. For this work, these packages have been bundled together in a software framework for evaluating various airfoils in different flight conditions and efficiently extract high level goal functions. These individual packages are explained first before the actual optimization is presented.

2.1 OPTIMIZATION STRATEGY

The underlying optimization strategy is based on the EGO algorithm by Jones et al. [32]. A design of experiment is carried out, where random designs are generated which are then evaluated with the simulation. Afterwards, a Kriging surrogate model [33] is built to approximate the functional behavior of the simulation. This surrogate is evaluated a lot faster than the simulation function and therefore enables the usage of global optimization technique which would otherwise be too expensive.

Here, the in-house Powerful Optimization Toolkit (POT) [34] is employed. In contrast to the initial perception by Jones et al. [32], it utilizes more recent design of experiment techniques and chains multiple optimization algorithms together to globally find the optimal solution with an accuracy of local searchers. Most noticeable, the Pareto front is searched using the Differential Evolutionary algorithm by Storn and Price [35], which has been extended to multi-objective problems using the sorting algorithm from the NSGA-II by Deb et al. [36]. With further enhancements, multiple goal functions as well as constraints can be handled. A technique coined 'crashmap' handles failing designs without tainting the original surrogate models with ill-posed penalty values.

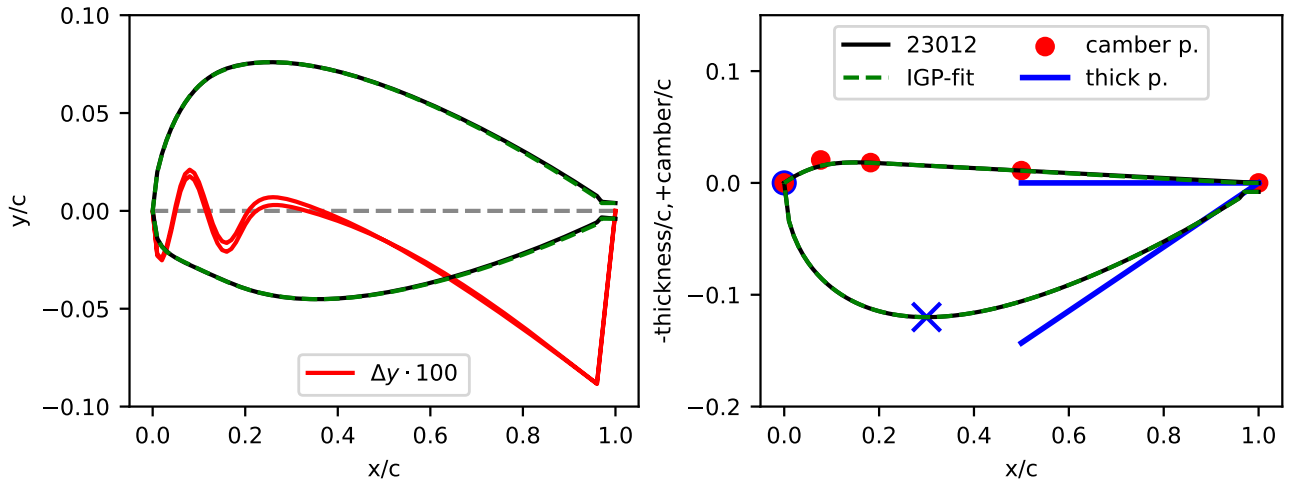

(a) Airfoil (b) Camberline and Thickness

Figure 1: Example parameterization of NACA23012 airfoil using the modified IGP method. camber .p shows the camberline control points and thick p. exemplary visualizes the thickness parameters

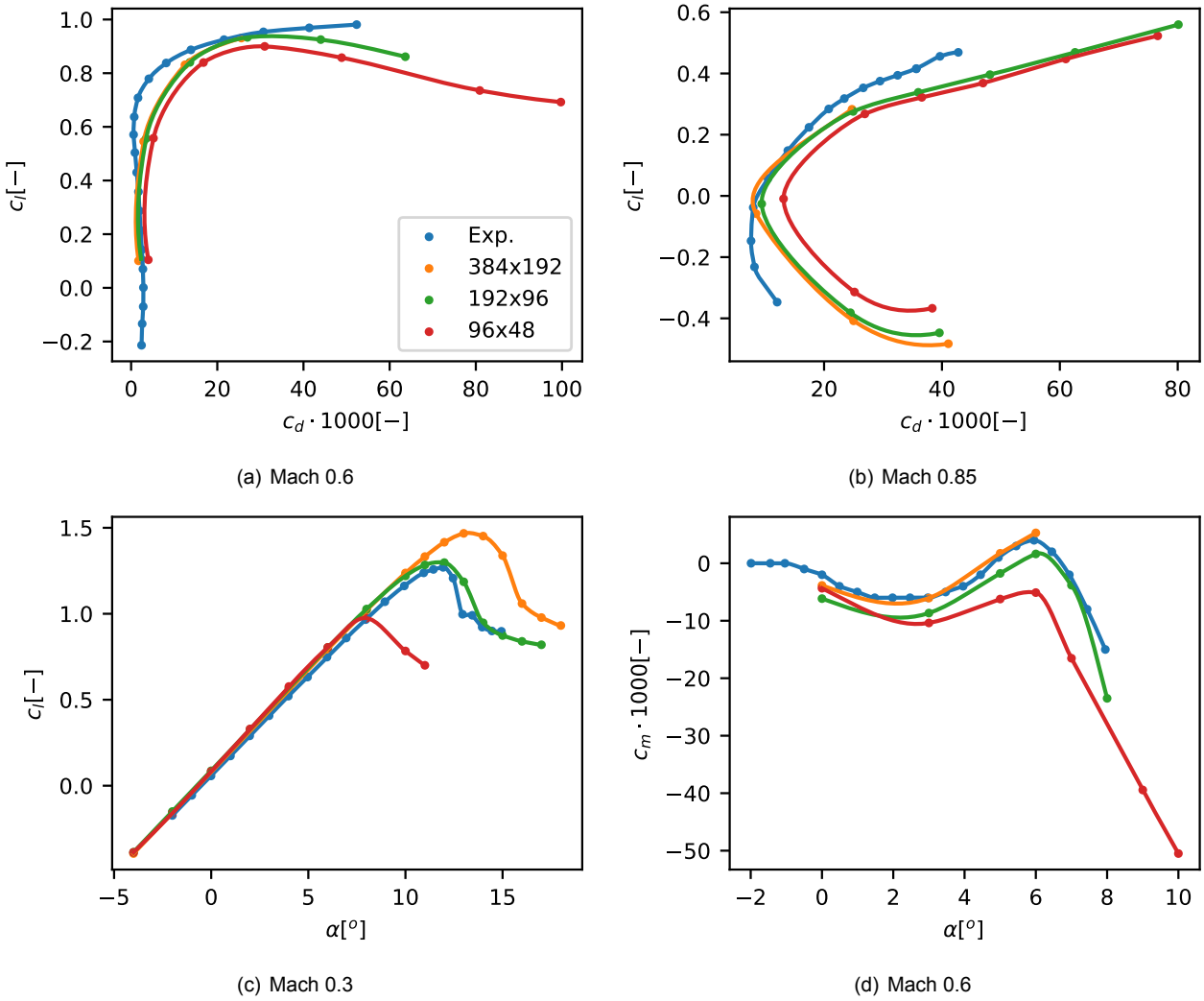

(a) Mach 0.6 (b) Mach 0.85

(c) Mach 0.3 (d) Mach 0.6

Figure 2: Validation of the DSA-9A airfoil simulations for various grid densities. Drag has been integrated from pressure only to match the experiment [37].

2.2 PARAMETERIZATION

While different techniques have been implemented, in this work the Improved Geometric Parameterization (IGP) proposed by Xiaoqiang et al. [11] is the underlying parameterization. It describes the airfoil through a parameterization of the camberline and a thickness distribution. The camberline is simply described through a Bezier spline with four control points, of which two control points may be freely moved in horizontal and vertical direction. The thickness distribution is based on the polynomial function also applied to the NACA 4 and 5 digit parameterizations [10]. Opposing the NACA parameterization, where only the maximum thickness may be varied, the IGP sets all five coefficients free. Through simple algebra they transform these to four parameters, which represent the nose radius of the airfoil ρ_0, the maximum thickness t and location of the maximum thickness x_t as well as the boat trailing edge angle β_{te}, i.e. the angle towards the closed leading edge. The beauty of this is that intuitive parameters are given for the thickness distribution.

The parameterization is somewhat modified as the camberline is simply parameterized with a spline using five controls points with three free control points. Since rotorcraft airfoils almost always feature a tab or blunt trailing edge, a simple function is superimposed to accommodate this. The thickness distribution is replaced with the tab thickness at an horizontal location equal to the chord length minus the trailing edge length. The camberline is then replaced with a linear function that allows to specify the tab trailing edge angle to further augment a potential reflex of the airfoils as required to keep the pitching moment within limits.

In Fig. 1, the tabbed NACA23012 airfoil as found on the HART-II rotor blade [38] is parameterized with the given method. The thickness distribution matches exactly due to the common definition, whereas a slight deviation of the camberline leads to an offset in the vertical direction towards the trailing edge and minor differences at the leading edge. This offset maybe further alleviated with more parameters for the camberline, but for these studies a total of five control points (10 parameters) is found to be acceptable.

2.3 SIMULATION

For the airfoil simulations, DLR's FLOWer code [40] is utilized. The flow solver is a block-structured multigrid solver. The airfoil simulations have been carried out using local time stepping with the SGS-Scheme [41] performing two stages and running a three stage multigrid cycle. The spatial discretization of the inviscid fluxes is based on the SLAU2 [42] scheme with a third order reconstruction [43], [44], whereas the turbulent fluxes used a first order reconstruction. The employed turbulence model is the Spalart-Allmaras [45] model. Transition is empirically predicted using the AHD criterion [46]. If a shock wave was present on either side of the airfoil, the transition location was set to the minimum pressure location to avoid numerical buffeting of the otherwise steady solution.

For the mesh generation, the in-house grid generator G^3 is employed which is based on transfinite interpolation [47]. A mesh sensitivity study of the applied O-grid has been carried with for the DSA-9A airfoil and is compared against the wind tunnel test [37], see Fig. 2. From the wind tunnel test matrix, two transonic flow conditions are selected roughly corresponding to the later used flow conditions for the optimization while while a low-speed flight condition is selected where later on the maximum lift coefficient is checked. The overall agreement with the wind tunnel is in good standing, yet towards larger lift coefficients a greater offset to the experiment is noticed, especially for the Mach 0.3 condition. On the CFD side, it is observed that the SA turbulence model is still very sensitive to the grid resolution near the stall, while on the other side, in the wind tunnel the experiment featured small dimensions and therefore blockage effects could not be fully avoided. Given that in the CFD setup, a plain free-stream airfoil is simulated in 2D fashion versus (corrected) 3D flow in the closed test section, the setup seems sufficiently reasonable for optimization. Klein et al. [48] have performed analysis with FLOWer that demonstrated that using a 3D setup will improve the correlation of (this) wind tunnel and CFD simulations. Yet, for design purposes, these setups would become to costly. From the investigated grid densities, the 192x96 setup is utilized as a fair trade-off between accuracy and speed. The drag and moment prediction is already close to the finest mesh result, while the too small maximum lift coefficient is considered acceptable as the differences between airfoils is captured.

For the later on applied rotor simulations, similar CFD parameters are utilized. However, a dual-time stepping approach is utilized along with the classical LU-SGS [49] scheme. The inviscid flux reconstruction is increased to 4th order, whereas the SA turbulence is enhanced through the rotation correction [50] and DDES [51] modifications. The simulations are then coupled with the comprehensive code HOST [52] by Airbus Helicopters to trim the rotor as well as to account for deformation. In forward flight, the Chimera technique is utilized and the ROTEST II fuselage from the HART-II campaign is included [38]. In hover, periodicity is assumed and only a single blade is simulated. Relatively coarse mesh setups have been generated for fast turnaround times and thus 2.2 million grid cells are used for the forward flight setup, whereas 670 thousand grid cells are used for the hover simulation. Nevertheless, when comparing

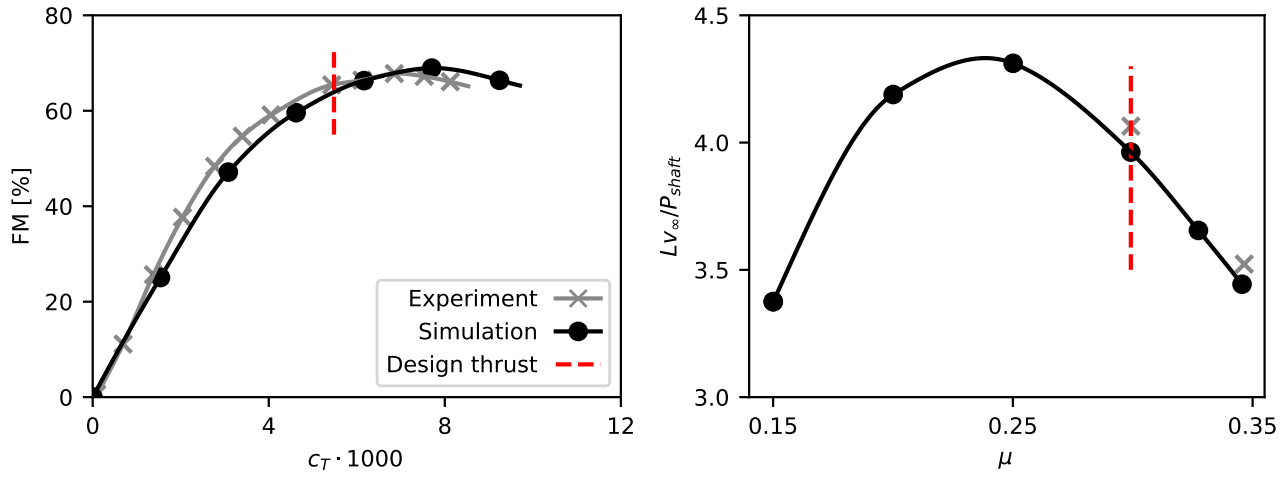

(a) Hover (b) Forward flight @ $c_T = 5.1/1000$

Figure 3: Validation of the rotor simulations in different flight conditions against FTK wind tunnel campaign results of the Bo-105 scaled rotor (aka HART-II) [39].

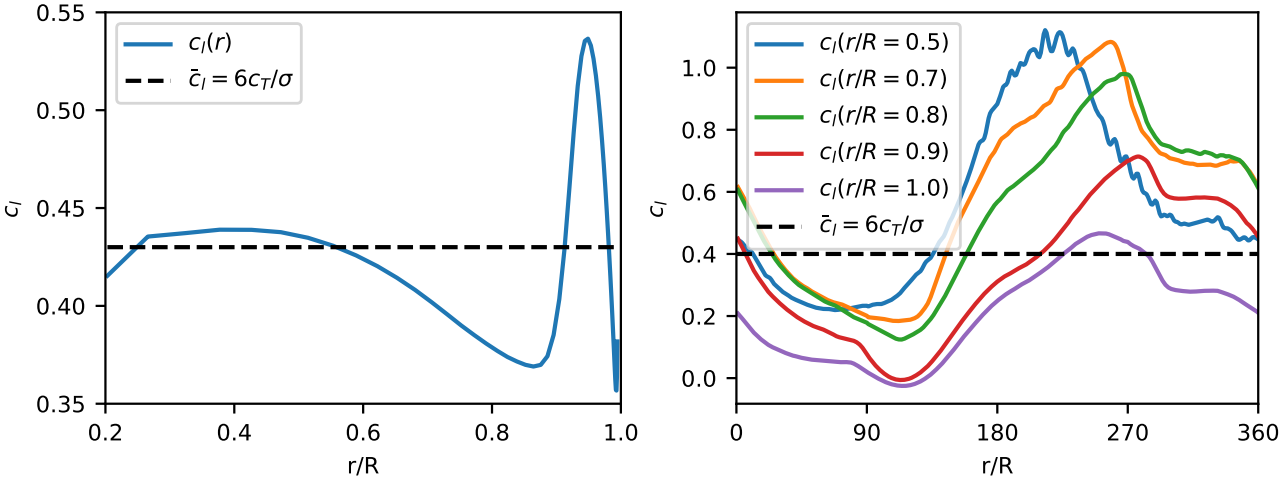

(a) Hover (b) Forward flight

Figure 4: Approximation of lift coefficients for the Bo105 scaled rotor in hover and forward flight.

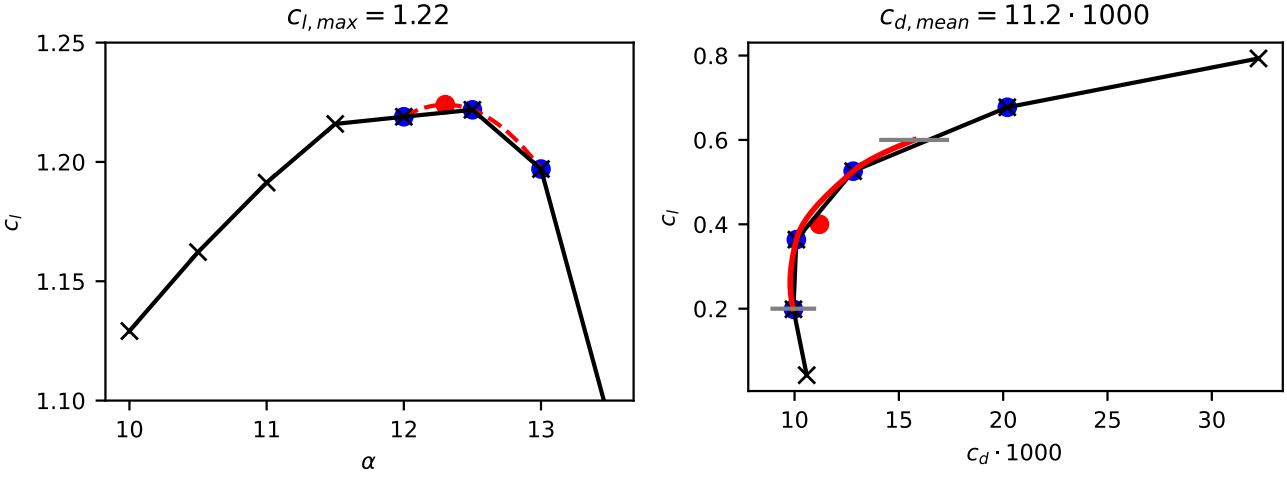

(a) maximum lift coefficient extraction (b) mean drag extraction

Figure 5: Sketch of the extraction of goal functions. The blue points represent the utilized data points, red lines the interpolation, and red points the final goal function value.

the results against the wind tunnel data of the scaled Bo105 rotor from the FTK campaign [39] in Fig. 3, the setups achieve a fair degree of accuracy deemed sufficient for checking the effect of modified airfoils.

3 OPTIMIZATION

3.1 TASK

The specified task is to improve the performance of the Bo105 scaled rotor, here synonymously referred to as HART-II rotor, by reducing the required power in hover as well as in forward flight. For hover, a thrust is set to $c_T = 5.5/1000$ and forward flight it is $c_T = 5.1/1000$ with an advance ratio of $\mu = 0.3$ as design conditions. One difficulty for the numerical optimization of airfoils is the specification of critical design conditions that represent the rotor flow. A simple estimation of the required lift coefficient c_l is given by $6 \cdot c_T/\sigma$ [53]. For the here chosen thrusts that would yield approximate lift coefficients of 0.43 and 0.40. However, modern rotors do not employ a single airfoil, nor is this brief representation sufficient to cover the whole range of lift coefficients the rotor encounters. In order to estimate the lift coefficients from a CFD simulation, the forces obtained from the simulation are used to estimate the inflow using a local momentum theory for the specific segment and simplifications regarding the total velocity V of the section:

$$c_l = c_z cos\phi - c_x sin\phi \tag{1}$$

$$\phi = arctan(v_i/V) \tag{2}$$

$$v_i \approx -\frac{v_\infty sin\alpha_q}{2} \pm \sqrt{|(\frac{v_\infty sin\alpha_q}{2})^2 + \frac{n_{blades} dF_z}{4\Pi\rho_\infty r dr}|} \tag{3}$$

$$V \approx \Omega r + v_\infty sin\psi \tag{4}$$

with $c_{x,z}$ the sectional coefficients in the rotating rotor mast system, ϕ the estimate induced inflow angle, v_i the induced velocity, v_∞ the forward flight velocity, n_{blades} the number of blades, ρ_∞ the free-stream density, r the radius of the section, Ω the rotational speed of the rotor and dF_z/dr the sectional force in the rotor mast direction. The results of the approximation are shown in Fig. 4. On the one hand, it is seen that the crude estimation for c_l with $6 \cdot c_T/\sigma$ would yield a good average, yet the variation of the lift coefficient c_l over the radius as well azimuth in forward flight is rather large. In hover, the incoming tip vortex from the previous blade causes a lowering of the lift coefficient on the downwash side, whereas it causes an overshoot on the upwash side. For the rotor in forward flight, the tip on the advancing side produces close to no lift, whereas the inboard retreating side sees lift coefficients of over one.

From both these flight conditions it is deduced that a rotor airfoil has to be designed for a very versatile flow environment stressing the statements regarding airfoil design by Dadone [3]. This is also a reason, why most modern helicopters employ multiple airfoils to tailor these to the specific needs. For this paper, three airfoils are designed. The first design simply tries to improve the NACA 23012 found on the HART-II rotor by replacing it with an optimized 12% thick airfoil. The second and third design are to be employed together in a combination of 12% and 9% thick airfoils. While thickness may be considered a design parameter, it is fixed here as it is usually constrained from a structural design perspective. Nevertheless, the combination of a thin and thick airfoil is not uncommon and can be found already on the 7A/D rotors [54], here 9% and 13% thickness. The general idea of employing thinner airfoils towards the tip is to decrease compressibility effects, especially occurring on the advancing side in forward flight. For a fair comparison, the 9% optimized airfoils are compared against a NACA 23009 airfoil with the same tab as found on the NACA23012 of the Bo105/HART-II rotor. The inboard airfoil runs up to r/R=80% and is then linearly transitioned into the outboard airfoil which then starts at r/R=90% and remains constant up to the tip.

12% only	Mach	Re x 10^6	c_l range
retreating	0.10	0.1	max
hover	0.65	1.9	0.2 ... 0.6
advancing	0.75	2.1	-0.2 ... 0.2
12% inboard	Mach	Re x 10^6	c_l range
retreating	0.10	0.1	max
hover	0.52	1.5	0.3 ... 0.6
advancing	0.75	2.1	-0.1 ... 0.3
9% outboard	Mach	Re x 10^6	c_l range
retreating	0.42	1.2	max
hover	0.65	1.9	0.2 ... 0.4
advancing	0.88	2.5	-0.2 ... 0.1

Table 1: Flight conditions for the various airfoil optimizations.

The optimization of the individual blades is thus split into looking at three different reference states that are loosely defined as retreating side, hover condition and advancing side and are listed for the three airfoil optimizations in Table 1. For all optimization, the following goal functions and constraints are imposed:

$$g_1(\vec{x}) = c_{d,hover,mean} \tag{5}$$

$$g_2(\vec{x}) = c_{d,adv,mean} \tag{6}$$

$$c_1(\vec{x}) = c_{l,ret,max} \tag{7}$$

$$c_2(\vec{x}) = |c_{m,hover}|_{mean} \tag{8}$$

Basically, the average drag in the hover and advancing side condition is to be minimized while the maximum lift coefficient is constrained as well as the

maximum absolute pitching moment. For the 12% thickness optimizations, a lift coefficient of 1.2 is to be reached, while it is 1.15 for the 9% optimization. The pitching moment constraint is 0.015 for the 12% only and 9% airfoil optimizations, while it is 0.02 for the 12% inboard optimization. For practical reasons, the extraction of goal functions is achieved by running a sweep over the angle of attack in each of the flight conditions and then interpolate 1001 intermediate values between the specified c_l ranges using modified Akima splines [55] to average c_d and $|c_m|$. For the extraction of $c_{l,max}$, a simple 2nd order polynomial is placed through the top three data points and through analytical derivation the peak value (and angle of attack) is found. The extraction of the maximum c_l and average drag $c_{d,mean}$ in hover is sketched in Fig. 5 for the NACA23012. During the data generation with CFD, a fixed number of iterations is run and the final convergence checked. The data point is rejected if the density residual has not dropped by four orders of magnitude. If for a given design, not enough data points exist for a specified flight condition, e.g. a too strong flow separation occurred and the requested c_l could not be reached, it is marked invalid and is not inserted into the surrogate model, but marked as a failed design in the 'crashmap'.

The parameters altered by the optimizers in this scenario are the nose radius ρ_0, the location of the maximum thickness x_t, the boat trailing edge angle β_{te}, the horizontal location of the third camberline control point x_3, the vertical locations of the second, third and fourth camberline control points y_{1-3} as well as the angle of tab θ_{tab}. The remaining parameters are set to the values found for the fit of the NACA23012 for the 12% airfoils, and the thickness t is set to 0.09 for the 9% airfoil. The leads to a total of eight design variables.

3.2 RESULTS

Since a multi-objective optimization is run, the Pareto fronts of the individual optimizations are shown in Fig. 6. The merits are scaled with respect to the results of the NACA23012 for the 12% optimizations and to the results of the NACA23009 for the 9% optimization. A general observation is that many tried samples violate the constraints and checking the Pareto optimal designs, most of them are close to violating the constraints. Also seeing points close to the Pareto front that seem to be Pareto optimal, but are disregarded due to constraint violations, leads to the conclusion that the optimization of rotor airfoils is very constraint driven. The 12% only optimization found 20 Pareto optimal designs, the 12% inboard optimization 11 Pareto optimal designs and the 9% outboard optimization 49 Pareto optimal designs. The overall number of tried designs is 1368, 1120 and 1351 re-

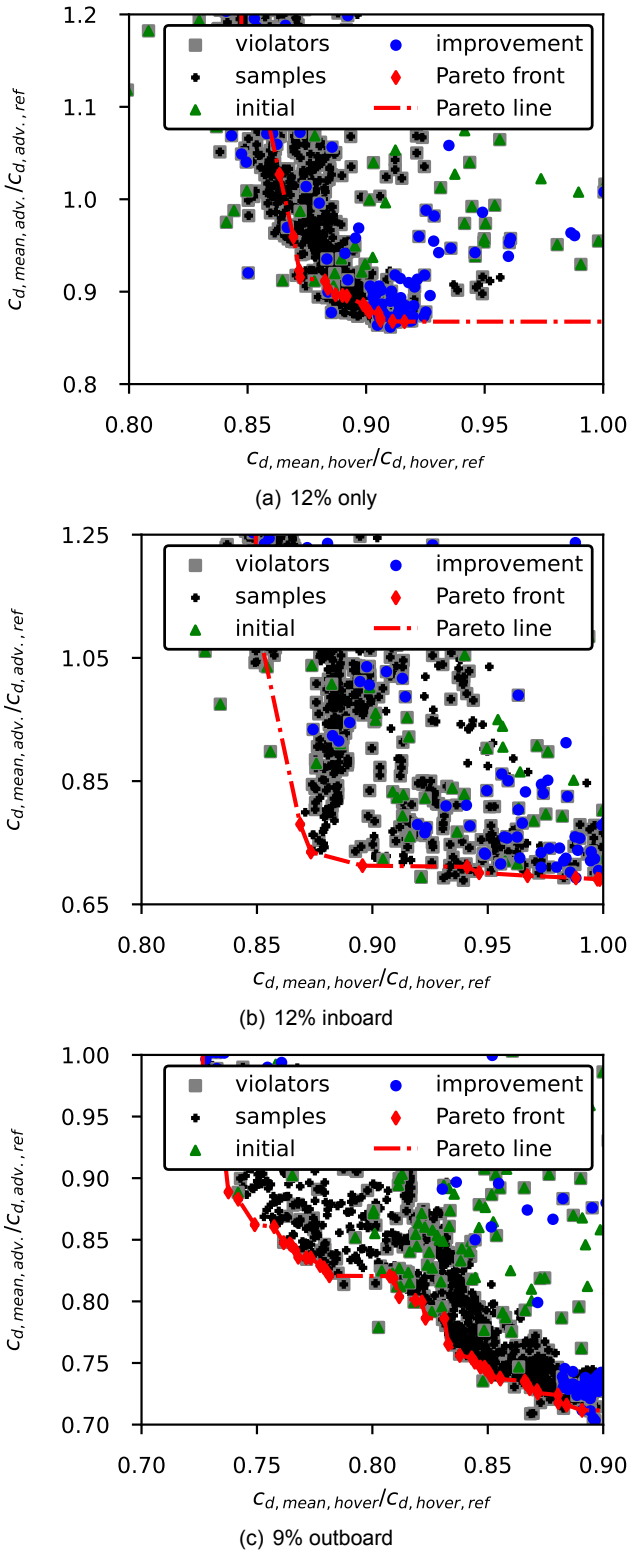

Figure 6: Pareto fronts obtained from the sampled designs. "initial" and "improvement" are samples from the Design of Experiments and the single-objective phase, the remaining samples are from the multi-objective phase. Violators are designs where the constraints have been violated.

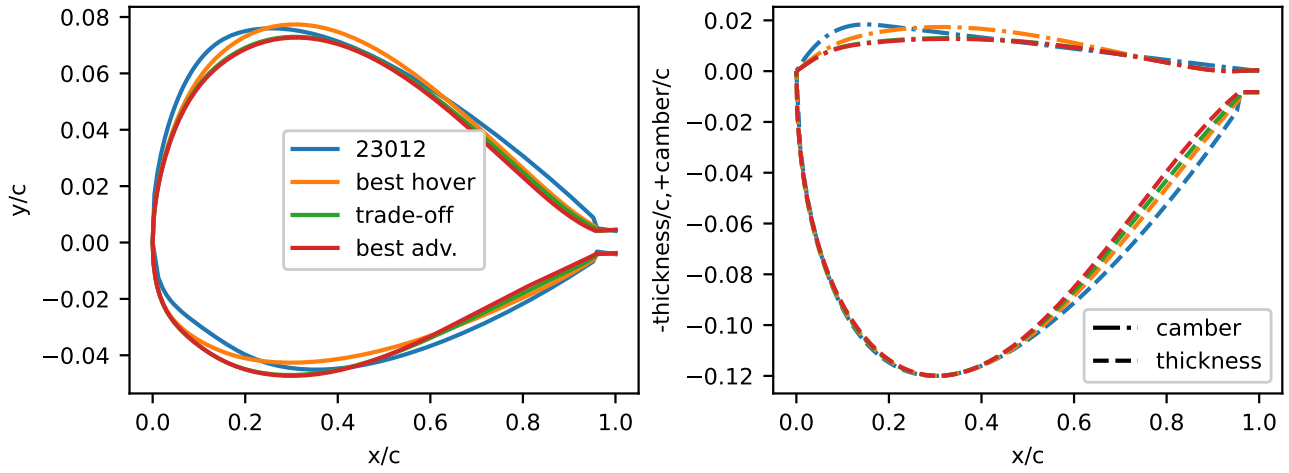

(a) Airfoil (b) Camberline and Thickness

Figure 7: Selected airfoil shapes from 12% only optimization

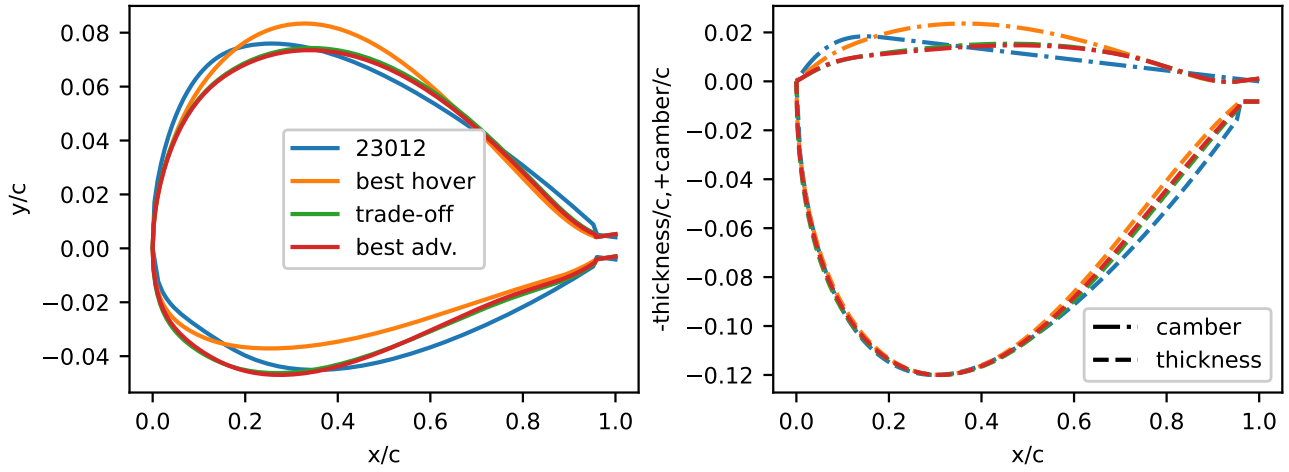

(a) Airfoil (b) Camberline and Thickness

Figure 8: Selected airfoil shapes from 12% inboard optimization

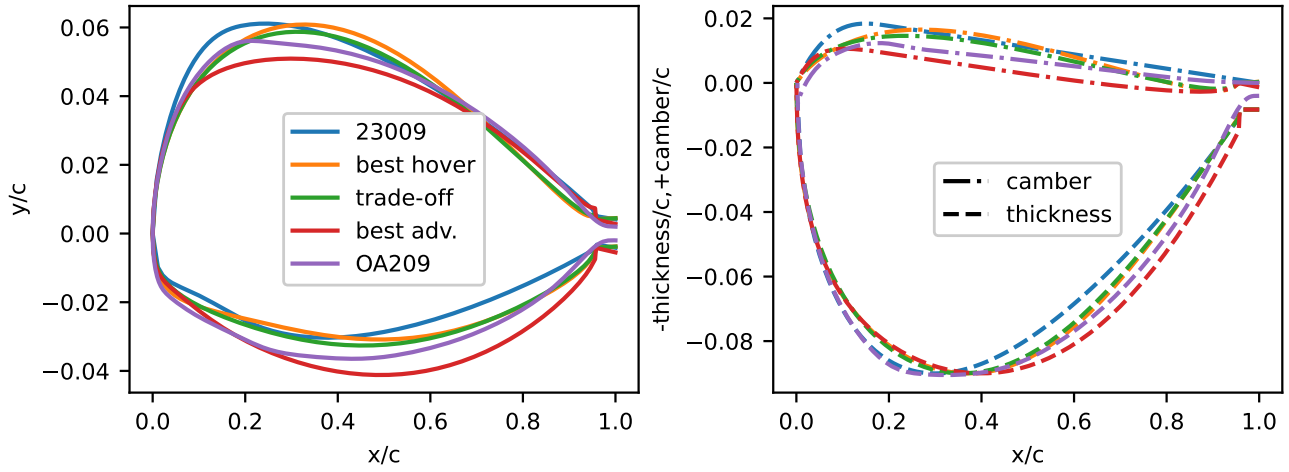

(a) Airfoil (b) Camberline and Thickness

Figure 9: Selected airfoil shapes from 9% outboard optimization

spectively.

The attainable merits for the 12% only optimization are a drag reduction of up to 15.3% for the hover condition and up to 13.2% in the advancing side conditions. These numbers are 15.0% and 31.0% for the 12% inboard optimization and 27.3% and 28.8% for 9% outboard optimization. Unfortunately, these are the numbers for one goal function of the anchor points and they cannot be achieved concurrently, thus they have to be traded in for one another.

3.3 SELECTED DESIGNS

From each optimization, three Pareto optimal design are chosen: the best hover design that still improves over the reference airfoil, the best advancing side design that still improves of the reference airfoil and an intermediate airfoil subjectively identified as a good trade-off design. In Fig. 7 to Fig. 9, the airfoil shapes as well the camberline and thickness distribution is plotted for these airfoils. For the 9% optimization results, the OA209 airfoil designed by Thibert and Gallot [4] is also plotted for reference. The common trend among the optimized airfoils is that the best hover airfoil features the greatest maximum camber, whereas the best advancing side airfoil the least camber with the trade-off design in-between. The location of the maximum camber is also further back for the optimized airfoils in comparison with the reference airfoils. The maximum thickness location remained around $x/c = 0.3$ for the 12% airfoils, but moves back for the 9% airfoils.

Moving over to the merits of these airfoils, in Fig. 10 to Fig. 12, the lift is plotted over the drag. For the 12% optimization, an overall improvement over a wide range of lift coefficients is found for the optimized shapes. The spread is little for the hover condition, but a more noticeable variation exists for the advancing side condition. Therefore, the best advancing side design is picked for further investigations on the Bo105 scaled rotor. For the 12% inboard optimization, the opposite is observed, where a more noticeable impact is seen in the hover condition, but a less pronounced impact in the advancing side condition. The reason for this are the different hover and cruise conditions from the 12% only conditions and are more specific to only find a suitable design for the inboard stations. Moving over to the 9% outboard optimization results, here a clear drag bucket build-up is seen for the best hover and trade-off designs with only a minor perception of this effect for the advancing side design and almost non-existent for the reference airfoil. The ranking of the airfoils then changes for the advancing side flight condition. Since the more specific optimization of the 12% inboard and 9% outboard optimizations show distinct designs for the various flight conditions, the selected trade-off airfoils are combined for the evaluation on the reference rotor. In contrast to the OA209 airfoil, which achieves quiet low drag coefficients in the hover condition, the trade-off design and the best hover design pose more robust designs for this flight condition as they offer this low drag over a wider range of lift coefficients. This is equally true for the advancing side condition, where all the optimized airfoils prevail over the OA209 for all lift coefficients.

Going deeper into the detail on why these airfoils improved, the pressure distributions from the selected designs are shown from Fig. 13 to Fig. 15 for the mean lift coefficient of the specific flow condition. For the hover condition, a constant and low pressure gradient helps in delaying the transition onset on the upper surface and thus improving the overall drag of the airfoil. For the advancing side cases, the occuring shock is the main driver and thus the optimizer tries to minimize the intensity of the shock to reduce the dominant wave drag. A potential seen for the parameterization of all optimizations is the transition to the tab, which may be accomplished more smoothly to avoid unnecessary kinks.

4 VERIFICATION OF ROTOR PERFORMANCE GAINS

The designs obtained from the 2D optimization proved their merits in their realm, yet they are to be tested on the real rotor. Therefore, the two sets of selected airfoils, the 12% only and the 12% inboard with the 9% outboard airfoil, are compared against the HART-II rotor, a modified HART-II rotor with NACA23009 at the outboard stations, and a modified HART-II rotor with the OA212 and OA209 airfoils. Later reflects slightly more recent airfoils, which are publicly available. Note that the airfoils have been aligned with their respective zero-lift angle-of-attack to avoid optimizing twist through differently cambered airfoils.

From these plots it is seen that exchanging the NACA23012 at the tip with the NACA23009 brought 1.5% improvement of the Figure of Merit at design thrust, whereas a power reduction of 1.0% is obtained in forward flight at the design flight condition. Further enhancing the HART-II rotor with the ONERA Airfoils delivers 1.8% improvement of the Figure of Merit and 1.9% power reduction in forward flight over the HART-II rotor. The gains are shifted for the 12% only optimized airfoil, which improves the Figure of Merit by 1.7% and reduces the required power in forward flight by 7.2%. The gain is further enhanced in the design flight conditions by 9/12% airfoil combination, where the Figure of Merit is increased by 2.1% and a power reduction of 8.6% is achieved in forward flight.

Additional observations are made: In hover, the improved airfoils deliver more gains at greater thrusts,

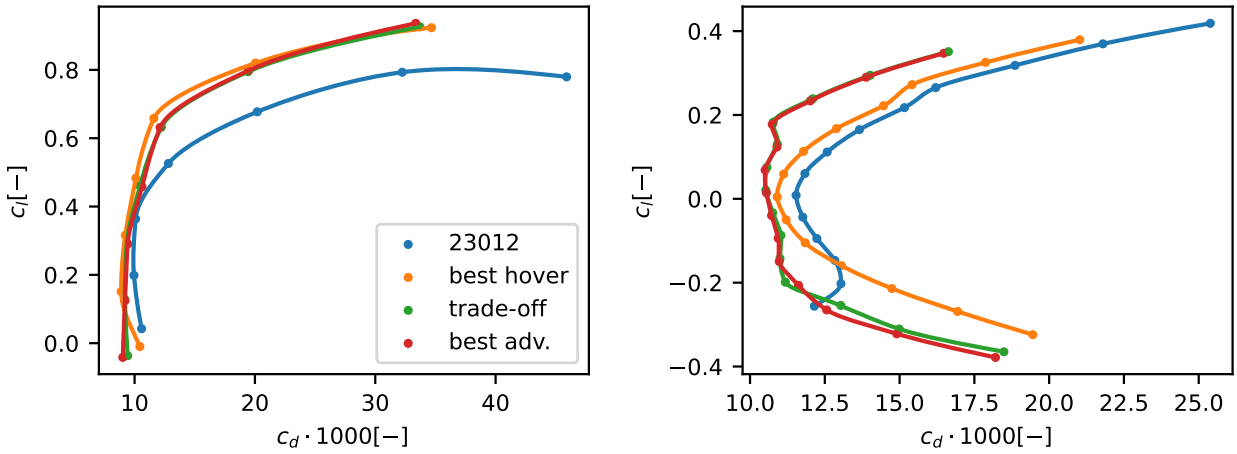

(a) hover condition (b) advancing side condition

Figure 10: Goal function data of selected airfoils from 12% only optimization

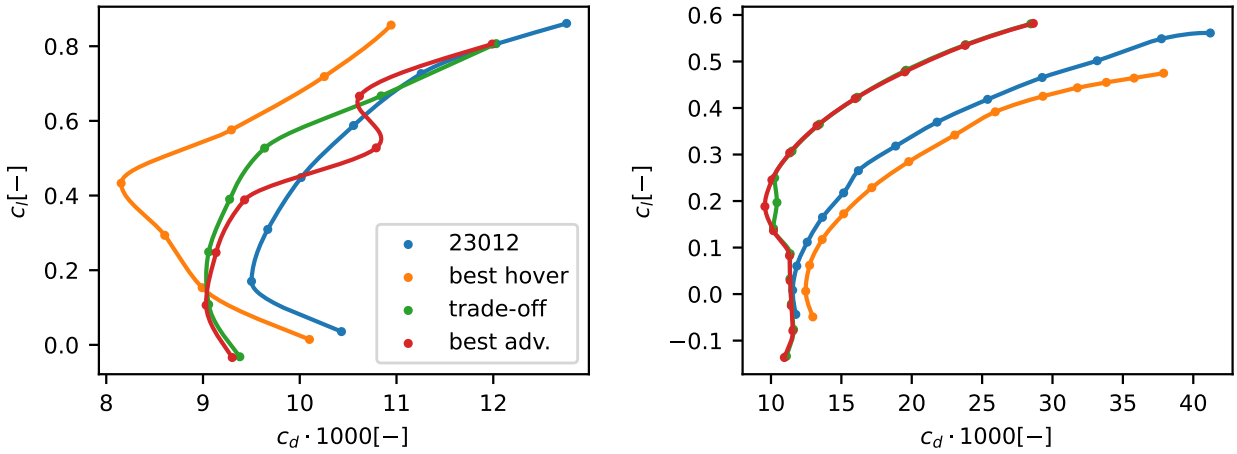

(a) hover condition (b) advancing side condition

Figure 11: Goal function data of selected airfoils from 12% inboard optimization

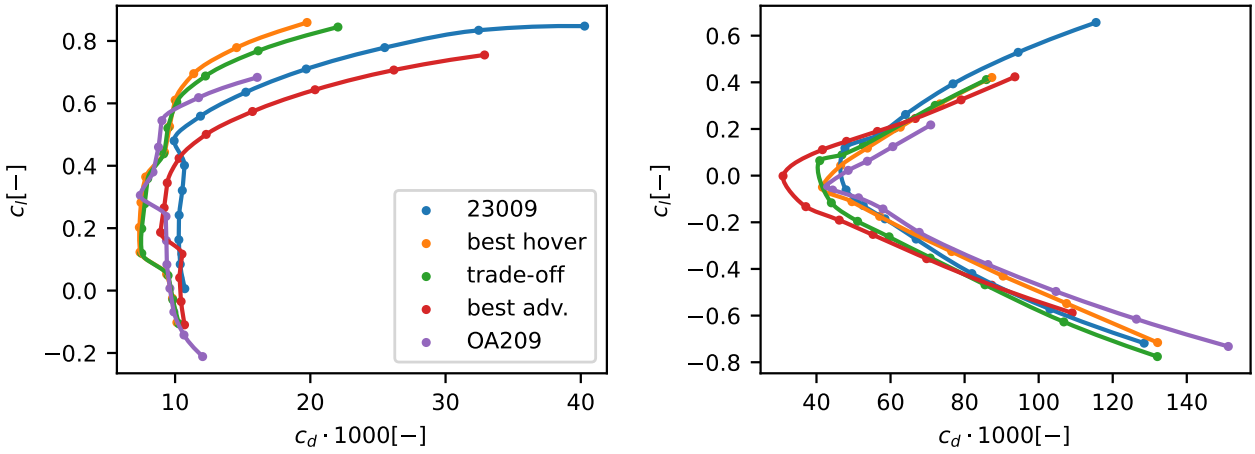

(a) hover condition (b) advancing side condition

Figure 12: Goal function data of selected airfoils from 9% outboard optimization

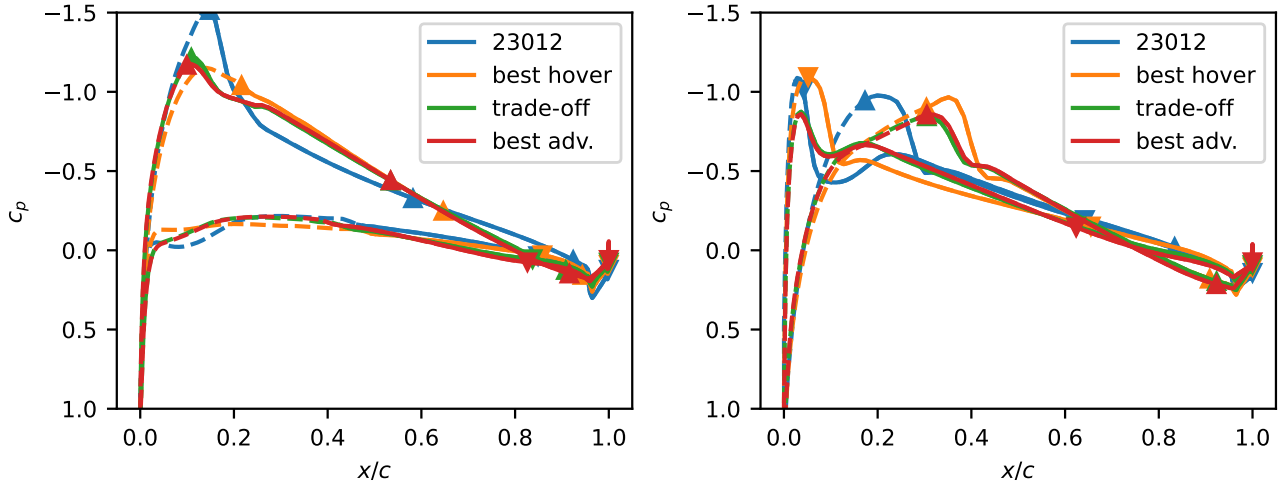

(a) hover condition ($c_l = 0.4$) (b) advancing side condition ($c_l = 0.0$)

Figure 13: Pressure distribution of selected airfoils from 12% only optimization. Dashed lines represent laminar regions. Δ is for the upper, and ∇ for the lower surface.

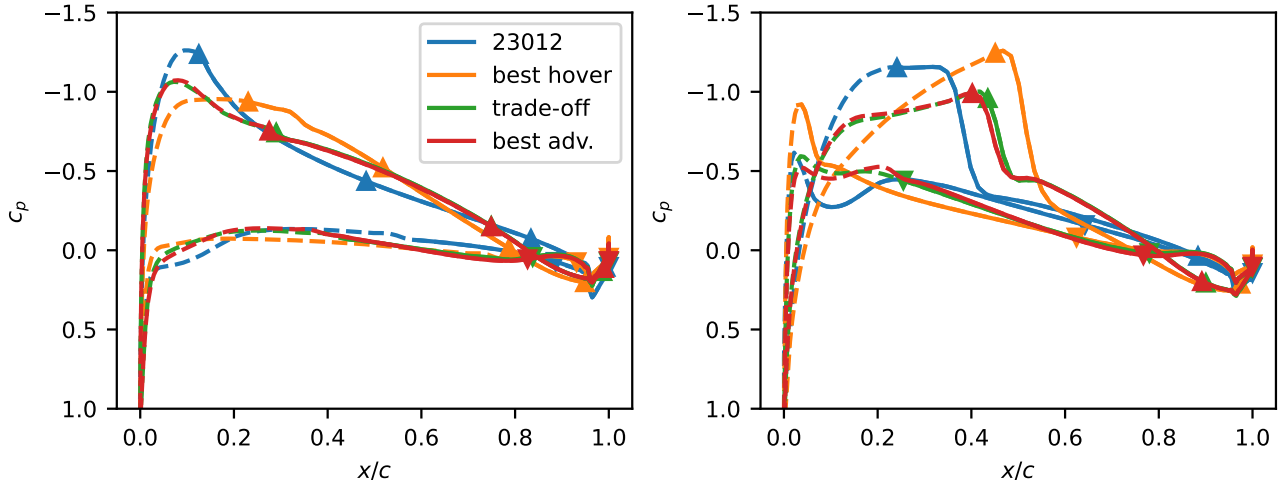

(a) hover condition ($c_l = 0.45$) (b) advancing side condition ($c_l = 0.1$)

Figure 14: Pressure distribution of selected airfoils from 12% inboard optimization. Dashed lines represent laminar regions. Δ is for the upper, and ∇ for lower the surface.

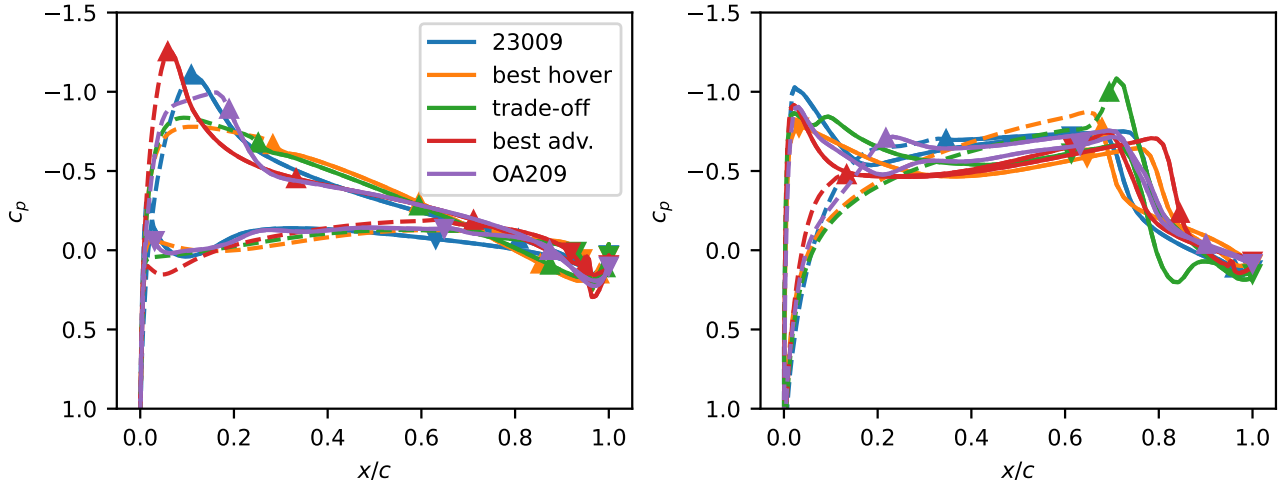

(a) hover condition ($c_l = 0.3$) (b) advancing side condition ($c_l = -0.05$)

Figure 15: Pressure distribution of selected airfoils from 9% outboard optimization. Dashed lines represent laminar regions. Δ is for the upper, and ∇ for the lower surface.

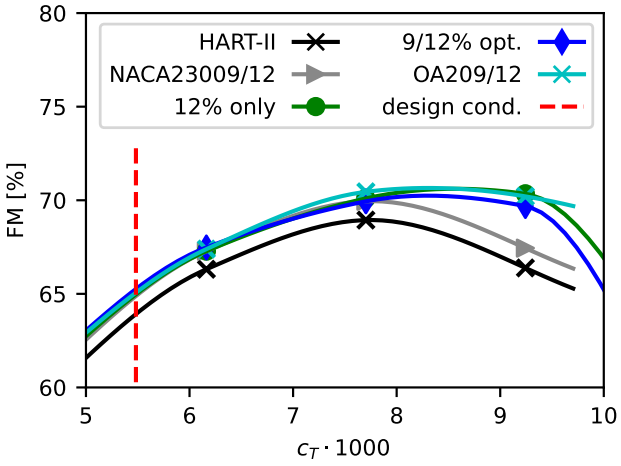

(a) Hover

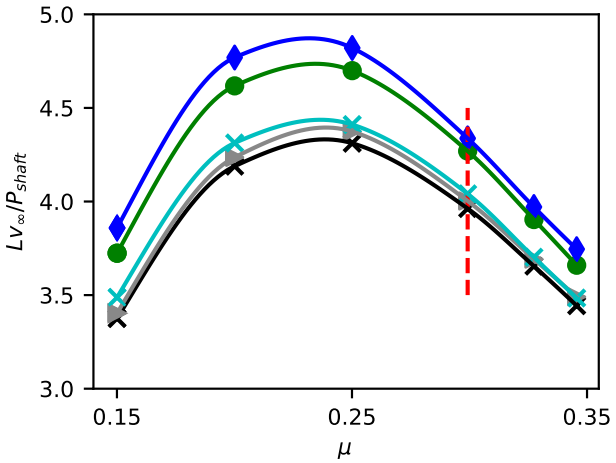

(b) Forward flight

Figure 16: Rotor performance of the optimized airfoils compared with reference airfoils.

while also being able to push the maximum computed thrust, here simulated in steps $\Delta c_T/\sigma = 0.02$, one step further. In forward flight, it is observed that all improved airfoils improve over the range of advance ratios, with the greatest gains at advance ratios around $\mu \approx 0.2$. The reason that the perceived gains are larger in forward flight than in hover are attributed to the fact that the relative induced power in hover is larger at higher thrusts than it is for the forward flight, where the induced power is lowest at the intermediate advance ratio of $\mu \approx 0.2$ for this rotor. The optimization of 2D sections of the rotor firstly allows to reduce the profile drag mostly associated with viscous forces. In forward flight, the wave drag may be partially reduced by reducing and improving the thickness distribution. However, the reduction of induced power may mostly be achieved through altering the lift distribution, which is more easily achieved through a twist & planform optimization. The gain of the 12% airfoil in hover at higher thrust is attributed to the delayed stall of the outboard station, which is the major driver to reduce the Figure of Merit at higher thrusts [56]. The stall behavior of the 9% airfoil is less suited in this flight condition.

5 SUMMARY

In this paper:

- A brief overview of the design approaches to finding new airfoil shapes have been reviewed along with long standing guidelines.
- A new framework for the optimization is proposed based on 2D numerical multi-objective optimizations. The major novelty is the application of the multi-objective optimization paradigm including aerodynamic design constraints to find designs suited for the variety of flight conditions a rotor blade section undergoes during operations. Minor adjustments to existing parameterizations were made to accommodate airfoil tabs, but also the application of third order CFD simulations brought progress in the accuracy of the results.
- The framework has been tested starting with simple but renowned and publicly available rotor and airfoil designs.
- The subset of the obtained airfoils has been further investigated in 3D rotor flow using coupled CFD/CSD simulations to validate the benefit of the 2D optimization for 3D rotor flows.

Findings from the investigations are:

- The design of a rotor airfoil is very constraints driven. While already discussed by for example Dadone [3] and by Thibert and Gallot [4] back in the 1970s, the fact remains true today. Allowing for greater margins for example in the pitching moment will allow to generate more lift with less drag. Obviously, this will come at a price of increasing the strength of the materials used on the rotor.
- The obtained airfoil designs were also able to surpass the designs by Thibert and Gallot [4]. One of the reasons is that a range of lift coefficients was required over a single lift coefficient. This, however, seems to be a possibility that becomes possible with the advent of large high-performance computing systems, which were not available back in 1977.
- For improving hover performance, maintaining a thicker airfoil over the whole blade proves beneficial, while for forward flight where shocks may

occur, a slimmer airfoil will help to alleviate wave drag

- The abstracted 2D flow conditions and optimizing over a range of lift coefficients instead of a single design point helped in delivering robust airfoils for a wider range of flight conditions of the rotor.

This approach and research may be extended to address:

- Inclusion of dynamic stall to avoid severe pitching moment stalls.
- Extension and examination of the effect of airfoils on rotor aero-acoustics.
- Potentially come up with an efficient 3D approach that allows the concurrent investigation of flight conditions. Preferably the planform & twist optimization is already included.

While the extensions should be straight forward, it is still a matter of resources and simulation efficiency will remain a key concern in numerical optimization.

References

[1] M. Drela: XFOIL: An analysis and design system for low Reynolds number airfoils. In: *Low Reynolds number aerodynamics*. Springer, 1989, S. 1–12

[2] M. Drela: *Two-dimensional transonic aerodynamic design and analysis using the Euler equation*, Massachusetts Institute of Technology. Department of Aeronautics and Astronautics, Dissertation, August 1986

[3] L. U. Dadone: Design and Analytical Study of a Rotor Airfoil / NASA. 1978 (Contractor Report 2988). – TechReport

[4] MM. J. J. Thibert, and J. Gallot: A New Airfoil Family for Rotor Blades. In: *Third European Rotorcraft Forum and Powered Lift Aircraft Forum*, 1977

[5] W. G. Bousman: Airfoil Design and Rotorcraft Performance. In: *58th Annual Forum of the American Helicopters Society*, 2002

[6] J. R. R. A. Martins, and A. Ning: *Engineering Design Optimization*. Cambridge University Press, 2021

[7] L. Piegl, and W. Tiller: *The NURBS Book (2nd Ed.)*. New York, NY, USA : Springer-Verlag New York, Inc., 1997. – ISBN 3–540–61545–8

[8] R. M. Hicks, and P. A. Henne: Wing Design by Numerical Optimization. In: *Journal of Aircraft* 15 (1978), Nr. 7, S. 407–412

[9] B. Kulfan: A Universal Parametric Geometry Representation Method - ”CST”. In: *45th AIAA Aerospace Sciences Meeting and Exhibit*, 2007

[10] C. L. Ladson, C. W. Brooks, Jr., A. S. Hill, and D. W. Sproles: Computer Program to Obtain Ordinates for NACA Airfoils / National Aeronautics and Space Administration. 1996 (4714). – Technical Memorandum

[11] L. Xiaoqiang, H. Jun, S. Lei, and L. Jing: An improved geometric parameter airfoil parameterization method. In: *Aerospace Science and Technology* 78 (2018), S. 241–247. – ISSN 1270–9638

[12] L. D. Allen, J. W. Lim, R. B. Haehnel, I. D. Dettwiller: Helicopter Rotor Blade Multiple-Section Optimization with Performance Considerations. In: *Proceedings of the 77th Annual Forum*. Virtual, May 2021

[13] In: H. Sobieczky: *Parametric Airfoils and Wings*. Wiesbaden : Vieweg+Teubner Verlag, 1999. – ISBN 978–3–322–89952–1, S. 71–87

[14] W. Song, and A. Keane: A Study of Shape Parameterisation Methods for Airfoil Optimisation. In: *10th AIAA/ISSMO Multidisciplinary Analysis and Optimization Conference*, 2004

[15] B. G. Marinus: Influence of Parameterization and Optimization Method on the Optimum Airfoil. In: *27th International Congress of the Aeronautics Sciences*, 2010

[16] C. Ilic, and J. Brezillon: Optimization of an airfoil polar in transonic RANS flow using an adjoint gradient-based approach. In: *15. STAB-Workshop*, 2011

[17] K. A. Lane: *Novel Inverse Airfoil Desing utlizing Parametric Equations*, California Polytechnic State University, San Luis Obispo, Masterstheses, 2010

[18] S. Obayashi and S. Takanashi: Genetic optimization of target pressure distributions for inverse design methods. In: *AIAA Journal* 34 (1996), Nr. 5, S. 881–886

[19] S. Koziel, and L. Leifsson†: Surrogate-Based Aerodynamic Shape Optimization by Variable-Resolution Models. In: *AIAA Journal* 51 (2013), S. 94–106

[20] L. Leifsson, S. Koziel, and Y. A. Tesfahunegn: Multiobjective Aerodynamic Optimization by Variable-Fidelity Models and Response Surface Surrogates. In: *AIAA Journal* 52 (2016), Nr. 2, S. 531–541

[21] A. Massaro, and A. D'Andrea: Multi-Point Aerodynamic Optimization by Means of Memetic Algorithm for Design of Advanced Tiltrotor Blades. In: *39th European Rotorcraft Forum*, 2013

[22] F. Fusi, A. Guardone, G. Quaranta, and P. M. Congedo: Multifidelity Physics-Based Method for Robust Optimization Applied to a Hovering Rotor Airfoil. In: *AIAA Journal* 53 (2015), Nr. 11, S. 3448–3465

[23] S. W. Lee, and O. J. Kwon: Aerodynamic Shape Optimization of Hovering Rotor Blades in Transonic Flow Using Unstructured Meshes. In: *AIAA Journal* 44-8 (2006), S. 1816–1825

[24] S. Choi , M. Potsdam, K. Lee, G. Iaccarino, and J. J. Alonso: Helicopter Rotor Design Using a Time-Spectral and Adjoint-Based Method. In: *12th AIAA/ISSMO Multidisciplinary Analysis and Optimization Conference 10 - 12 September 2008, Victoria, British Columbia Canada*, 2008

[25] L. Wang, B. Diskin, R. T. Biedron, E. J. Nielsen, and O. A. Bauchau: Evaluation of High-Fidelity Multidisciplinary Sensitivity-Analysis Framework for Multipoint Rotorcraft Optimization. In: *Journal of Aircraft* 57 (2020), Nr. 5, S. 830–842

[26] E. Fabiano, A. Mishra, D. Mavriplis, and K. Mani: Time-dependent Aero-acoustic Adjoint-based Shape Optimization of Helicopter Rotors in Forward Flight. In: *57th AIAA/ASCE/AHS/ASC Structures, Structural Dynamics, and Materials Conference, AIAA SciTech Forum*, 2016

[27] N. A. Vu, H.-J. Kang, A. I. Azamatov, J.-W. Lee, and Y.-H. Byun: Aerodynamic Design Optimization of Helicopter Rotor Blades in Hover Performance using Advanced Configuration Generation Method. In: *35th European Rotorcraft Forum*, 2009

[28] N. A. Vu and J. W. Lee: Aerodynamic design optimization of helicopter rotor blades including airfoil shape for forward flight. In: *Aerospace Science and Technology* 42 (2015), S. 106–117. – ISSN 1270–9638

[29] V. Ahuja, C. Kannepalli, A Zambon, H. Lapin, and Mark Potsdam: Unsteady Blade Shape Optimization for Rotorcraft. In: *70th Annual Forum of the American Helicopters Society*, 2014

[30] K. Mani, B. A. Lockwood, and D. J. Mavriplis: Adjoint-based Unsteady Airfoil Design Optimization with Application to Dynamic Stall. In: *68th Annual Forum of the American Helicopters Society*, 2012

[31] A. D. Gardner, K. Richter, H. Mai, A. R. M. Altmikus, A. Klein, and C.-H. Rohardt: Experimental Investigation of Dynamic Stall Performance for the EDI-M109 and EDI-M112 Airfoils. In: *Journal of the American Helicopter Society* 58 (2013), Nr. 1, S. 1–13. – ISSN 2161–6027

[32] D. R. Jones, M. Schonlau, and W. J. Welch: Efficient Global Optimization of Expensive Black-Box Functions. In: *Journal of Global Optimization* 13 (1998), S. 455–492

[33] D. Krige: *A statistical approach to some mine valuation and allied problems on the Witwatersrand*, University of the Witwatersrand, Dissertation, 1951

[34] G. Wilke: Variable-Fidelity Methodology for the Aerodynamic Optimization of Helicopter Rotors. In: *AIAA Journal* 57 (2019), Nr. 8, S. 3145–3158

[35] R. Storn, and K. Price: Differential Evolution - A simple and efficient adaptive scheme for global optimization over continuous spaces. In: *Journal of Global Optimization* 11 (1997), S. 341–359

[36] K. Deb, A. Pratap, S. Agarwal, and T. Meyarivan: A fast and elitist multiobjective genetic algorithm: NSGA-II. In: *IEEE Transactions on Evolutionary Computation* 6 (2002), Nr. 2, S. 182–197. – ISSN 1089–778X

[37] K. Richter, C. C. Wolf, A. Gardner, and C. B. Merz: Detection of Unsteady Boundary Layer Transition Using Three Experimental Methods. In: *54th AIAA Aerospace Sciences Meeting*

[38] B. G. van der Wall: A Comprehensive Rotary-Wing Data Base for Code Validation: The HART II International Workshop. In: *The Aeronautical Journal* 115 (2011), Nr. 1164, S. 91–102

[39] P. Küfmann, R. Bartels, B. G. van der Wall, O. Schneider, H. Holthusen, J. Gomes, and J. Postma: The First Wind Tunnel Test of the DLR's Multiple Swashplate System: Test Procedure and Preliminary Results. In: *AHS 72nd Annual Forum*, 2016

[40] J. Raddatz, and J. K. Fassbender: Block Structured Navier-Stokes Solver FLOWer. In: Kroll, Norbert (Hrsg.) ; Fassbender, Jens K. (Hrsg.): *MEGAFLOW - Numerical Flow Simulation for Aircraft Design*. Berlin, Heidelberg : Springer Berlin Heidelberg, 2005. – ISBN 978–3–540–32382–2, S. 27–44

[41] D. Sharov, H. Luo, J. Baum, and R. Loehner: Implementation of unstructured grid GMRES+LU-SGS method on shared-memory, cache-based parallel computers. In: *38th Aerospace Sciences Meeting and Exhibit*, 2000

[42] K. Kitamura, and E. Shima: Towards shock-stable and accurate hypersonic heating computations: A new pressure flux for AUSM-family schemes. In: *Journal of Computational Physics* 245 (2013), S. 62–83. – ISSN 0021–9991

[43] S. Yamamoto, S. Kano, and H. Daiguji: An Efficient CFD Approach for Simulating Unsteady Hypersonic Shock-Shock Interference Flows. In: *Computers & Fluids* 27 (1998), Nr. 5, S. 571–580. – ISSN 0045–7930

[44] G. Wilke: Comparisons of Different Spatial Schemes and Limiters for Helicopter Flows. In: A. Dillmann, G. Heller, E. Krämer, and C. Wagner (Hrsg.): *New Results in Numerical and Experimental Fluid Mechanics XIII*, Springer International Publishing, 2021. – ISBN 978–3–030–79561–0, S. 418–427

[45] S. Allmaras, F. T. Johnson, and P. Spalart: Modifications and clarifications for the implementation of the Spalart-Allmaras turbulence model. In: *Seventh International Conference on Computational Fluid Dynamics (ICCFD7),*. Big Island, Hawaii, January 2012, S. 1–11

[46] D. Arnal, R. Houdeville, A. Seraudie, and O. Vermeersch: Overview of laminar-turbulent transition investigations at ONERA Toulouse. In: *41st AIAA Fluid Dynamics Conference and Exhibit*, 2011

[47] C. B. Allen: CHIMERA volume grid generation within the EROS code. In: *Proceedings of the Institution of Mechanical Engineers, Part G: Journal of Aerospace Engineering* 214 (2000), 125–140

[48] A. Klein, Th.Lutz, E.Krämer, K. Richter, A. D. Gardner, and A. R. M. Altmikus: Numerical Comparison of Dynamic Stall for Two-Dimensional Airfoils and an Airfoil Model in the DNW–TWG. In: *Journal of American Helicopter Society* (2012)

[49] S. Yoon, and A. Jameson: Lower-upper Symmetric-Gauss-Seidel method for the Euler and Navier-Stokes equations. In: *AIAA Journal* 26 (1988), Nr. 9, S. 1025–1026

[50] J. Dacles-Mariani, D. Kwak, and G. Zilliac: On numerical errors and turbulence modeling in tip vortex flow prediction. In: *International Journal for Numerical Methods in Fluids* 30 (1999), Nr. 1, S. 65–82

[51] P. R. Spalart, S. Deck, M. Shur, K. D. Squires, M. Kh. Strelets, and A. Travin: A New Version of Detached-eddy Simulation, Resistant to Ambiguous Grid Densities. In: *Theoretical and Computational Fluid Dynamics* 20 (2006), May, Nr. 3, 181. – ISSN 1432–2250

[52] B. Benoit, A.-M. Dequin, K. Kampa, W. von Grünhagen, P.-M. Basset, and B. Gimonet: HOST, a General Helicopter Simulation Tool for Germany and France. In: *56th Annual Forum of the American Helicopters Society*. Virginia Beach, VA, May 2000

[53] J. G. Leishman: *Principles of Helicopter Aerodynamics*. Cambridge University Press, 2006

[54] M. Allongue and J.P. Drevet: New rotor test rig in the large Modane wind tunnel. In: *15th European Rotorcraft Forum*. Amsterdam, NL, 1989

[55] Cosmin Ionita: *Makima Piecewise Cubic Interpolation*. website https://blogs.mathworks.com/cleve/2019/04/29/makima-piecewise-cubic-interpolation/. Version: April 2019

[56] G. Wilke, J. Bailly, Joëlle, K. Kimura, and Y. Tanabe: JAXA-ONERA-DLR cooperation: results from rotor optimization in hover. In: *CEAS Aeronautical Journal* (2022), S. 1–21. – ISSN 1869–5582